AIAA JOURNAL
Vol. 47, No. 6, June 2009

Application of Proper Orthogonal Decomposition to Trailing-Edge Noise

Stewart A. L. Glegg*
Florida Atlantic University, Boca Raton, Florida 33431
and
William J. Devenport† and Nicolas Spitz‡
Virginia Polytechnic Institute and State University, Blacksburg, Virginia 24061

DOI: 10.2514/1.41921

This paper demonstrates the calculation of airfoil trailing-edge noise from detailed models of the turbulent velocity fluctuations in the trailing-edge boundary layer. Velocity fluctuations are specified in terms of a set of statistically independent modes, each of which can be used independently to initiate a model for the convection of vorticity past the trailing edge. The acoustic radiation from each mode can then be computed, and the statistics of the far-field sound can be obtained from the independent sum of each modal contribution. Details of the approach are provided and a sample calculation is performed using proper orthogonal modes obtained from a direct numerical simulation of a turbulent boundary-layer flow. Comparison with experimental data shows the resulting noise predictions to be reasonably accurate. An analysis of the prediction shows that most of the noise is produced by large-scale streamwise velocity modes in the bottom 10% of the boundary layer.

Nomenclature

a_n	=	stochastic random variables
C_{ij}	=	velocity cross spectrum
c_o	=	speed of sound
$Ex[\,]$	=	expected value
k	=	magnitude of wave number $\lvert\mathbf{k}\rvert$
$\mathbf{k}$	=	wave number vector
L	=	wetted semispan
M_o	=	Mach number of the flow outside the boundary layer
M_v	=	Mach number of the local flow
M_w	=	W/c_o
M_{or}, M_{vr}, M_{wr}	=	components of the Mach numbers M_o, M_v, and M_w in the direction of the observer
$p(\mathbf{x}, t)$	=	fluctuating pressure
Q	=	source term, units of velocity squared
$\mathbf{q}$	=	vorticity of unsteady flow
r_e	=	propagation distance from source to observer
S_{pp}	=	far-field sound spectrum
s_i	=	unsteady velocity integrated over the span
T	=	averaging time
t	=	time
$\mathbf{U}(\mathbf{y})$, $U_i(\mathbf{y})$	=	mean velocity
$\mathbf{u}(\mathbf{y}, t)$, $u_i(\mathbf{y}, t)$	=	velocity perturbation $\mathbf{u} = \mathbf{v} - \mathbf{U}$
$V(y_2)$	=	mean convection velocity in boundary layer, $V = U_1(y_2)$
$\mathbf{v}(\mathbf{y}, t)$, $v_i(\mathbf{y}, t)$	=	total velocity $\mathbf{v} = \mathbf{U} + \mathbf{u}$
W	=	mean convection velocity in wake
$\mathbf{x}$, x_i	=	position vector of observer
$\mathbf{y}$, y_i	=	position vector of source
α	=	observer angle in the x_2, x_3 plane
θ	=	observer angle from the x_1 axis
$\lambda_\omega^{(n)}$	=	variance of a_n
ρ_o	=	density
σ	=	$W/V(y_2)$
Ω	=	mean vorticity
ω	=	angular frequency

I. Introduction

MANY approaches have been used to define the mechanisms of trailing-edge noise. For example, Ffowcs Williams and Hall [1] derived a theory based on the solution to Lighthill's wave equation, using a Green's function, which allowed for the scattering of flow noise by a semi-infinite half-plane. Amiet [2,3] derived a trailing-edge noise theory based on the scattering of airfoil surface pressure fluctuations produced by turbulent eddies as they convect past the trailing edge. In contrast, Howe [4] reformulated the acoustic analogy so that edge noise could be related to the vorticity in the boundary layer. He identified the importance of applying the Kutta condition and considered how individual vortex elements convect, causing vortex shedding at the trailing edge. These studies [4] have shown that the modeling has a significant impact on the predicted levels of radiated sound. Howe [5] also reduces his theory to a form which relates the blade surface pressure spectrum to the acoustic field, and has applied this to broadband noise calculations.

The turbulent boundary layer has a stochastic nature that confounds simple analytical treatment. As a consequence, the measured blade surface pressure spectrum (Howe [5], Glegg and Jochault [6]) has become the preferred input for calculations of broadband trailing-edge noise. However, to achieve a better understanding of the mechanisms involved, models based on the boundary-layer vorticity and its evolution past the trailing edge are very attractive. Recent developments in the application of proper orthogonal decomposition to aeroacoustics give new insights into the structure of turbulent flow, which can be applied to this problem [7–10] and have allowed the far-field sound to be related to an optimal modal decomposition of the

Presented as Paper 2911 at the AIAA/CEAS 10th Aeroacoustics Conference, Manchester, England, U.K., 10–12 May 2004; received 30 October 2008; revision received 13 February 2009; accepted for publication 14 February 2009.

*Professor, Department of Ocean Engineering, Center for Acoustics and Vibration. Associate Fellow AIAA.

†Professor, Department of Aerospace and Ocean Engineering. Associate Fellow AIAA.

‡Graduate Research Assistant, Department of Aerospace and Ocean Engineering; currently Boeing Commercial Airplanes, Seattle, Washington. Member AIAA.

turbulent flow. Using this approach, the turbulence can be described in terms of a set of statistically independent velocity modes, each of which can be used independently to initiate a model for the aeroacoustic source terms. The calculation of the acoustic radiation from each mode can then be computed, and the statistics of the far-field sound can be obtained from the independent sum of each modal contribution (Glegg and Devenport [7]). In this paper, details of a calculation are provided that demonstrate how data from a direct numerical simulation (Moser et al. [11]) of turbulent boundary-layer velocity fluctuations can be used to calculate far-field trailing-edge noise. The results of this calculation are compared with experimental measurements of noise from an isolated airfoil in a wind tunnel by Brooks et al. [12].

II. Trailing-Edge Noise Modeling

Consider a boundary layer flowing over the trailing edge of a flat plate with the coordinate system shown in Fig. 1. The mean flow will be assumed to be two-dimensional with no flow along the edge, and so $\mathbf{U} = (V(y_2), 0, 0)$. Following Howe [4], it is assumed that the vorticity is convected by the local mean flow and remains undistorted in the vicinity of the edge. In addition, there is vorticity shed into the wake, which is convected with the wake convection speed W, and its strength is determined by the application of the Kutta condition. Howe [4] gives the acoustic far field for an observer at $\mathbf{x}$ in the $x_3 = 0$ plane as

$$p(\mathbf{x},\omega) = \frac{\rho_o \sin(\theta/2) e^{i\omega(r_e - x_1 M_o)/c_o}}{i\omega r_e (1 + M_{or})(1 - M_{wr})} \times \int_0^\infty \frac{\sqrt{M_v}(1-\sigma) Q(\mathbf{k}, y_2) e^{-|\omega| y_2 / V(y_2)}}{\sqrt{2}(1 - M_{vr})(1 - M_v)^{1/2}} \, \mathrm{d}y_2 \tag{1}$$

where $M_o = U/c_o$ is the Mach number of the flow outside the boundary layer, $M_v = V(y_2)/c_o$ is the Mach number of the local flow, W is the mean convection velocity in the wake, and $M_w = W/c_o$. The Mach numbers M_{or}, M_{vr}, and M_{wr} are the components of the Mach numbers in the direction of the observer. The coefficient σ determines the effect of the Kutta condition and is defined as $\sigma = W/V(y_2)$. The source term Q is given by

$$Q(\mathbf{k}, y_2) = \frac{1}{(2\pi)^2} \int_{-\infty}^{\infty}\int_{-\infty}^{\infty} \mathbf{k} \cdot [\mathbf{q} \times \mathbf{U}]_{t=0} e^{-ik_1 y_1 - ik_3 y_3} \, \mathrm{d}y_1 \, \mathrm{d}y_3 \qquad \mathbf{k} = (\omega/V, -i|\omega|/V, 0) \tag{2}$$

where $\mathbf{q}$ is the vorticity of the unsteady flow. Howe's [4] result can be extended to include the effect of mean flow shear by adding $\boldsymbol{\Omega} \times \mathbf{u}$ to the term in square brackets. Assuming that the turbulent velocity fluctuations in the boundary layer are well modeled at low Mach numbers by an incompressible flow represented by $\mathbf{u}^{(L)}$ gives

$$Q(\mathbf{k}, y_2) = \frac{1}{(2\pi)^2} \int_{-\infty}^{\infty}\int_{-\infty}^{\infty} \left[\frac{-i|\omega|\Omega_3 u_1^{(L)} - \omega \Omega_3 u_2^{(L)}}{V(y_2)} - i|\omega| \left(\frac{\partial u_2^{(L)}}{\partial y_1} - \frac{\partial u_1^{(L)}}{\partial y_2} \right) \right]_{t=0} e^{-ik_1 y_1} \, \mathrm{d}y_1 \, \mathrm{d}y_3 \tag{3}$$

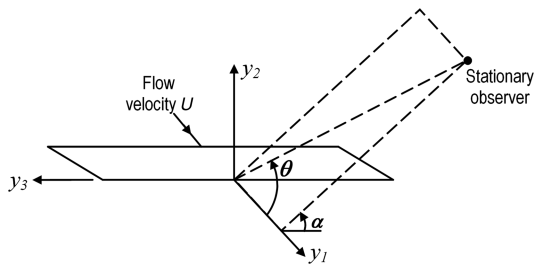

Fig. 1 Coordinate system used in the analysis of trailing-edge noise.

Assuming the turbulence is frozen and convects with the mean flow, evaluation of the integral over y_1 at fixed time is equivalent to an integral over time at a fixed location $y_1 = d$. This implies that the change in eddy motion is small compared to the eddy speed. Thus,

$$Q(\mathbf{k}, y_2) = \frac{-1}{(2\pi)^2} \int_{-\infty}^{\infty}\int_{-\infty}^{\infty} \left[-\Omega_3 (i|\omega| u_1^{(L)} + \omega u_2^{(L)}) - i|\omega| \left(-\frac{\partial u_2^{(L)}}{\partial t} - V(y_2) \frac{\partial u_1^{(L)}}{\partial y_2} \right) \right]_{y_1 = d} e^{i\omega t} \, \mathrm{d}t \, \mathrm{d}y_3 \tag{4}$$

It is convenient to introduce a spanwise integral of the unsteady velocity $s_i(y_2, \omega)$, which is a random stochastic variable defined as

$$s_i(y_2, \omega) = \frac{1}{2\pi L} \lim_{k_3 \to 0} \int_{-L}^{L}\int_{-\infty}^{\infty} [u_i^{(L)}(\mathbf{y}, t)]_{y_1 = d} e^{i\omega t - ik_3 y_3} \, \mathrm{d}t \, \mathrm{d}y_3 \tag{5}$$

where $2L$ is the wetted span of the plate, and the integral over y_3 is the wave number transform of the velocity perturbation across the span, evaluated at zero wave number. Equation (4) then becomes

$$Q(\mathbf{k}, y_2) = \frac{L}{2\pi} \left[\Omega_3 (i|\omega| s_1 + \omega s_2) + i|\omega| \left(i\omega s_2 - V(y_2) \frac{\partial s_1}{\partial y_2} \right) \right] \tag{6}$$

Defining the far field by using Eq. (6) in Eq. (1) reveals how the source term can be calculated directly from the velocity spectrum of the unsteady flow. In a potential mean flow, this calculation only depends on the unsteady vorticity, and so has the advantage that acoustic perturbations in the unsteady flow are eliminated. However, the evaluation of derivatives of the unsteady flow can cause numerical error, so if Eq. (4) or Eq. (6) are used in Eq. (1), integration by parts may be the correct approach to minimize numerical error in the evaluation of the integral over y_2. If it is assumed that there is no mean shear, then the integration is straightforward and gives

$$p(\mathbf{x},\omega) \approx -\frac{\rho_o \sin(\theta/2) e^{i\omega(r_e - x_1 M_o)/c_o}}{i\omega r_e (1 + M_{or})(1 - M_{wr})} \frac{\sqrt{M_v}(1-\sigma)|\omega| L}{2\pi\sqrt{2}(1 - M_{vr})(1 - M_v)^{1/2}} \times \int_0^\infty (i|\omega| s_1 + \omega s_2) e^{-|\omega| y_2 / V(y_2)} \, \mathrm{d}y_2 \tag{7}$$

III. Far-Field Spectra for Broadband Noise

To evaluate the far-field sound spectrum, it is assumed that the velocity fluctuations $u_i^{(L)}$ are a statistically stationary process with a two-point correlation function between velocities at $\mathbf{y}$ and $\mathbf{y}'$, defined as $R_{ij}(\mathbf{y}, \mathbf{y}', \tau)$. By taking the Fourier transform of the cross-correlation function with respect to time, the cross-spectral density $C_{ij}(\mathbf{y}, \mathbf{y}', \omega)$ is obtained. This can be used to specify the proper orthogonal modes of the flow as the solutions to an eigenvalue problem (see Glegg and Devenport [7]).

Using this approach, the spanwise integral of the unsteady velocity can be expressed as the sum of a set of orthogonal modes $s_i^{(n)}(y_2, \omega)$ as

$$s_i(y_2, \omega) = \sum_{n=1}^{\infty} a_n(\omega) s_i^{(n)}(y_2, \omega) \tag{8}$$

where the coefficients a_n are a set of uncorrelated stochastic random variables with zero mean and for which the variance is equal to $\lambda_\omega^{(n)}$.

The modes are defined by the solution to the eigenvalue problem

$$\begin{aligned}&\frac{1}{R}\int_0^R C_{ij}^{(1)}(y_2, y_2', \omega) s_j^{(n)}(y_2', \omega)\, \mathrm{d}y_2' \\ &\quad = \frac{\pi}{T}\lambda_s^{(n)} s_i^{(n)}(y_2, \omega) \quad \text{with} \quad C_{ij}^{(1)}(y_2, y_2', \omega) \\ &\quad = \frac{\pi}{TL^2}\int_{-L}^{L}\int_{-L}^{L} Ex[u_i^{(L)}(y_2, y_3, \omega)^* u_j^{(L)}(y_2', y_3', \omega)]\, \mathrm{d}y_3'\, \mathrm{d}y_3 \\ &\quad = \frac{\pi}{TL}\int_{-L}^{L} Ex[u_i^{(L)}(y_2, 0, \omega)^* u_j^{(L)}(y_2', \Delta y_3, \omega)]\, \mathrm{d}(\Delta y_3) \end{aligned} \tag{9}$$

where T is the averaging time used in the statistical estimate, and the calculation has been simplified by assuming that the flow is homogeneous in the spanwise direction.

Using Eq. (8) in Eq. (1) gives the acoustic pressure as

$$p(\mathbf{x}, \omega) = \sum_{n=1}^{\infty} a_n(\omega) p^{(n)}(\mathbf{x}, \omega) \tag{10}$$

where

$$\begin{aligned}p^{(n)}(\mathbf{x}, \omega) &= \frac{\rho_o \sin(\theta/2) e^{i\omega(r_e - x_1 M_o)/c_o}}{i\omega r_e (1 + M_{or})(1 - M_{wr})} \\ &\times \int_0^{\infty}\left(\frac{\sqrt{M_v}(1-\sigma) Q^{(n)}(\mathbf{k}, y_2) e^{-|\omega| y_2 / V(y_2)}}{\sqrt{2}(1 - M_{vr})(1 - M_v)^{1/2}}\right)\mathrm{d}y_2 \end{aligned} \tag{11}$$

and the source term is defined as

$$\begin{aligned}Q^{(n)}(\mathbf{k}, y_2) = \frac{1}{2\pi}\Bigg[&\Omega_3 (i|\omega| s_1^{(n)} + \omega s_2^{(n)}) \\ &+ i|\omega|\left(i\omega s_2^{(n)} - V(y_2)\frac{\partial s_1^{(n)}}{\partial y_2}\right)\Bigg]_{y_1 = d}\end{aligned} \tag{12}$$

The two-sided spectral density of the pressure fluctuations in the acoustic far field can then be obtained as

$$S_{pp}(\mathbf{x}, \omega) = \frac{\pi}{T} Ex[|p(\mathbf{x}, \omega)|^2] = \frac{\pi}{T}\sum_{n=1}^{\infty} \lambda_{\omega}^{(n)} |p^{(n)}(\mathbf{x}, \omega)|^2 \tag{13}$$

The advantage of this approach is that the noise generation associated with each mode can be identified and related to specific regions of the flow. In the following sections, this procedure is demonstrated and the new insight it provides is discussed.

IV. Modeling the Flow

To perform a noise calculation requires knowledge of the two-point cross spectrum of the turbulent boundary-layer velocity fluctuations passing the trailing edge. To provide this information with the minimum of empirical input requires a direct numerical simulation (DNS) solution of the flow. A noise calculation based on such a solution provides a means to validate the noise model and can give some physical insight into those aspects of the flow that are most responsible for producing the noise.

The source terms for a noise calculation have been extracted from the DNS solution of Moser et al. [11]. This solution is for a fully developed two-dimensional channel flow boundary layer at a Reynolds number of 590, based on the channel half-height and friction velocity U_τ. Channel flow simulations are available to higher Reynolds numbers than external boundary-layer simulations because a straightforward temporal solution can be performed using periodic grids in the streamwise direction. It is generally accepted that channel and external boundary-layer flows are similar in the inner region [13]. There are differences, of course, in the outer part of the layer and on scales of the order of the boundary-layer thickness [14]. In the inner region, recent work by Monty et al. [15] has shown that the characteristic spanwise lengthscale of structures in the near-wall region of a channel flow is about 1.6 times that in a boundary layer. This difference should be kept in mind when interpreting the present results.

The solution of Moser et al. [11] was calculated on a grid consisting of 384 equally spaced streamwise positions, extending over a length of $2\pi\delta$, and the same number of spanwise points equally spaced over a distance of $\pi\delta$. A total of 257 points were distributed according to a cosine function in the normal-to-wall y_2 direction, with the greatest resolution at the two channel walls. Figure 2 shows mean velocity and turbulence kinetic energy profiles at the computed resolution. The grid spacing is about half a wall unit at $y^+ = 1$, and there are 36 points within the bottom 10% of the channel half-height. These results have been previously analyzed by a number of workers (see references in Moser et al. [11]) and are an AGARD test case for the validation of large-eddy simulation solutions (Jimenez [16]).

Some 34 snapshots of the instantaneous velocity field of the flow at the computed resolution, Fourier transformed in the streamwise and spanwise directions, were provided by Moser et al. [11]. The snapshots represented irregularly spaced time intervals and thus could not be used to directly infer time delay correlations or frequency spectra. Instead, the Fourier transformed velocity fields were multiplied and averaged to yield the two-wave-number cross spectrum of the flow,

$$\Theta_{ij}(k_1, y_2, y_2', k_3) = \frac{\pi^2}{L_x L_z} Ex[u_i^*(k_1, y_2, k_3) u_j(k_1, y_2', k_3)] \tag{14}$$

where L_x and L_z are the half-length and half-width of the computational domain. To make this calculation practical, the cross spectrum was only stored for every fourth y_2 location over half the channel height and for a roughly exponentially distributed set of wave numbers in the streamwise and spanwise directions. The exponential distribution preserved the wave number resolution at the lowest wave numbers as well as three-quarters of the wave number range with a 10:1 reduction in the number of wave number values. The resulting interpolated data set appeared to resolve all the statistical features of the original data. Applying Taylor's hypothesis to relate streamwise wave number to frequency, that is, setting $\omega = -V_c k_1$ where V_c is the mean boundary-layer convection speed, the spanwise-averaged cross spectrum required for Eq. (9) was obtained from Θ_{ij} as

$$C_{ij}^{(1)}(y_2, y_2', \omega) = \frac{2\pi}{LV_c}\Theta_{ij}(\omega, y_2, y_2', 0) \tag{15}$$

where, as before, $2L$ is the wetted span of the trailing edge. The zero wave number velocity modes of Eq. (9) were computed using a standard matrix decomposition routine. For this computation, $C_{ij}^{(1)}$ was linearly interpolated to a 100×100 point grid of evenly spaced

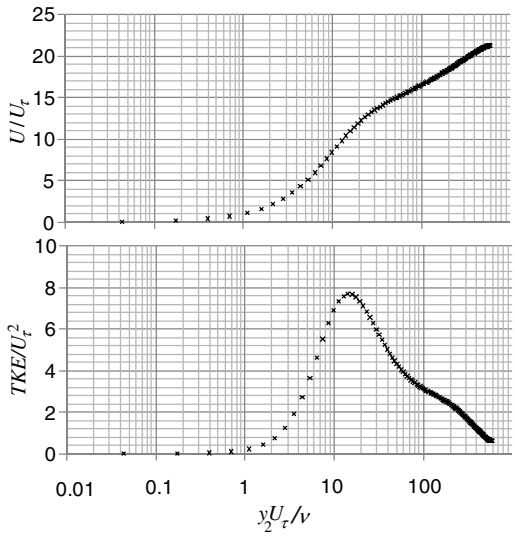

Fig. 2 Mean velocity and turbulence kinetic energy (TKE) profiles from the DNS simulation of Moser et al. [11].

(y_2, y_2') values extending from the wall to the boundary-layer edge. (Grid independence was established by repeating calculations on 200×200 and 400×400 point grids.) The computed eigenvalues and mode shapes were then used in a straightforward manner to compute the source terms of Eq. (12) and the acoustic pressure terms of Eq. (10) for each mode at each frequency. The derivative appearing in Eq. (12) was computed by first-order central difference. The integral in Eq. (10) was computed as a simple summation. The mean velocity and vorticity distributions required in Eq. (12) were obtained from reduced data files provided with the DNS solution. At every stage of this calculation (the computation of the velocity modes, the corresponding source modes, and the integrand of the acoustic pressure terms), the first four modes were plotted at every frequency and examined to verify adequate resolution and the absence of other numerical problems.

V. Comparison with Experiment

To complete the DNS-based calculation and provide a basis for comparison, a test case for the noise prediction was chosen from the study of Brooks et al. [12]. Specifically, run 295 of their study was chosen, which is for a tripped 0.1016-m chord, 0.457-m span NACA 0012 airfoil at zero angle of attack in a flow of 39.6 m/s. Being tripped and at zero angle of attack, the trailing-edge boundary layers are presumably fully turbulent and symmetric, and the trailing-edge boundary-layer thickness Reynolds number $U_1\delta/\nu$ is close to 15,000. This is quite a good match to the DNS, for which the equivalent Reynolds number is almost 13,000.

Brooks et al. [12] present far-field noise spectra for an observer positioned perpendicular to and 1.22 m from the trailing edge at midspan ($\theta = 90$ deg, $r_e = 1.22$ m). The density and sound speed were taken as 1.1 kg/m^3 and 340 m/s, respectively. The trailing-edge boundary-layer thickness (needed to scale the DNS modes) was taken as the measured value of close to 5.7% chord. The wake and average boundary-layer convection velocities W and V_c were taken as $0.6U$. Predictions were doubled to account for the boundary layers on both sides of the trailing edge.

Single-sided one-third octave band sound pressure level (SPL) spectra are presented in Fig. 3. Noise predictions based on the DNS source terms are compared with Brooks et al.'s [12] measured spectrum and curve fit starting at the lowest frequencies resolved in the DNS. It is important to emphasize that the predictions presented in Fig. 3 involve no empirical information connecting the boundary-layer properties to the far field or to the unsteady pressure around the trailing edge. Given this, the predictions come surprisingly close to the measurements. For frequencies over 3 kHz, the predictions are within 3 dB of the measurement and curve fit. There is even some suggestion that they reproduce the change in slope of the measured spectrum between 5 and 6 kHz.

At most points below 3 kHz, the predictions lie about 5 dB below the measurements. There may be a logical explanation here. The first four spectral points in the prediction are at frequencies that correspond to the longest streamwise lengthscales computed in the DNS, with wavelengths of $2\pi/\delta$, π/δ, $2\pi/3\delta$, and $\pi/2\delta$. These are the wavelengths that will be most affected by the periodicity condition used in the DNS and that would also be least representative of the turbulence in an external boundary-layer flow. Whether or not this is the explanation, it is interesting that such low-frequency boundary-layer motions contribute to the noise peak.

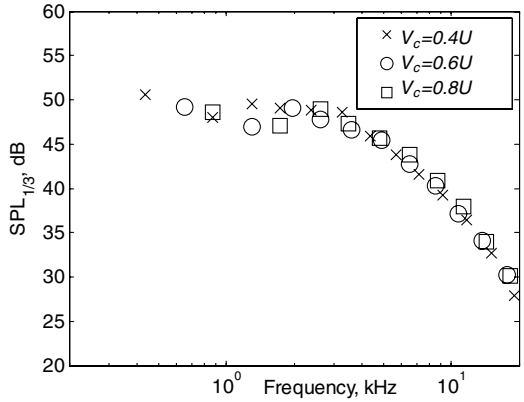

Fig. 4 Insensitivity of the computed noise levels to the choice of convection speed $V_c = W$.

One possible shortcoming of the prediction based on DNS source terms is the arbitrary nature of the choice of convection speed in both boundary layer and wake and the related applications of Taylor's hypothesis. Figure 4, however, shows that this may not be a big factor, especially at frequencies above 2 kHz. Spectra predicted using convection speeds of $0.4U$, $0.6U$, and $0.8U$ are compared here. Changing the convection speed of course changes the frequency associated with the DNS source terms but, despite this, has a surprisingly weak effect on the level and shape of the spectrum.

VI. Noise Contributions

The realism of the prediction based on the DNS source terms provides some justification for decomposing the predicted noise levels to reveal those features and parts of the boundary-layer flow that contribute most to the far-field noise. Three different decompositions are considered here: by the terms contributing to the total source $Q^{(n)}$ in Eq. (12), by the proper orthogonal mode numbers, and by location in the boundary layer.

Consider the four terms comprising the right-hand side of Eq. (12):

$$\underbrace{i\Omega_3|\omega|s_1^{(n)}}_{\text{term1}} \underbrace{+\Omega_3\omega s_2^{(n)}}_{\text{term2}} \underbrace{-|\omega|\omega s_2^{(n)}}_{\text{term3}} \underbrace{-i|\omega|V(y_2)\frac{\partial s_1^{(n)}}{\partial y_2}}_{\text{term4}} \qquad (16)$$

Terms 1 and 2 represent contributions from streamwise and normal to wall velocity fluctuations. Terms 3 and 4 represent the con-

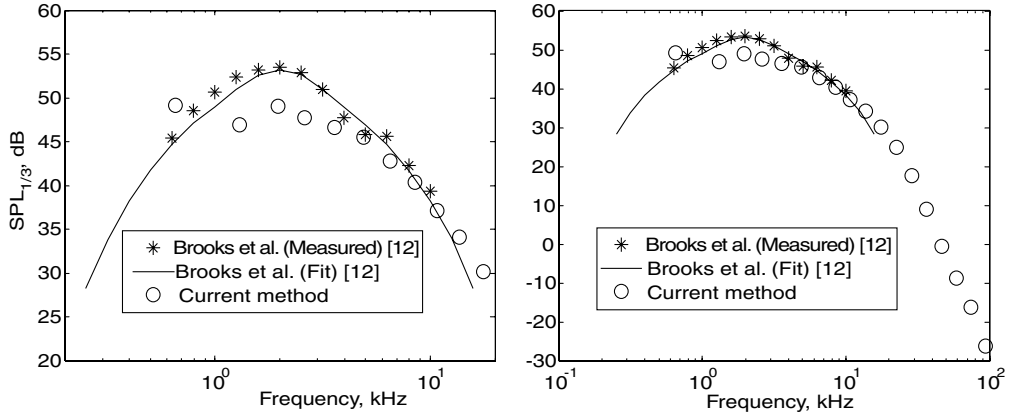

Fig. 3 Far field trailing-edge noise spectra from Brooks et al. [12], run 295, compared with predictions made using the current method with source terms computed from a DNS solution for $V_c = W = 0.6U$. The two plots show different frequency ranges.

tributions of these velocities to the spanwise vorticity fluctuation. Figure 5a shows the noise predicted separately from each of these terms compared with the total noise. Note that the contributions from the terms do not add to the total because the cross products between them, which result from the squaring that occurs in Eq. (13), are not included. The magnitude of these terms is shown in Fig. 5b. Figure 5a shows the streamwise velocity terms 1 and 4 are the dominant contributors. The normal-to-wall velocity term 2 is negligible (despite the large mean vorticity) and the associated vorticity term 3 is only a small contributor. The cross terms are small but there are nonnegligible contributions from the products between terms 1 and 4, 3 and 4, and 1 and 2.

Figure 6 shows contributions to the noise from the five most dominant modes at each frequency. Note that the modes at each frequency are ordered by the magnitude of their contribution to the noise, and thus the decay with increase in mode number is guaranteed. However, it is interesting to note that this ordering is not much different than that based on the eigenvalues of the cross spectrum $C_{ij}^{(1)}$. That is, the dominant modes of the cross-spectrum function tend also to be the dominant noise producers. Figure 7 shows the cumulative contributions to the overall sound pressure level from the modes. This plot shows that only the first five or six modes at each frequency are needed to give an overall SPL within 1 dB of the total predicted level.

Figure 8 shows the predicted noise spectrum divided up by location in the boundary layer. The figure shows the noise spectra predicted when the integration in Eq. (10) is carried out over slices one-tenth of the boundary-layer thickness in size. Note that the sum of the contributions is not quite the total noise because the division does not include the cross products between the contributions, which arise from the squaring in Eq. (13). These cross products are negligible except at the lower frequencies (<4 kHz). Here, contributions are in most cases positive for adjacent locations but negative for positions separated by 20–30% of the boundary-layer thickness.

Overall though, it is clear that the bulk of the predicted noise results from source terms lie in the bottom 10% of the boundary layer. Mathematically, this is because of the dominance of the exponential weighting function in the integrand of Eq. (10). Physically, this result

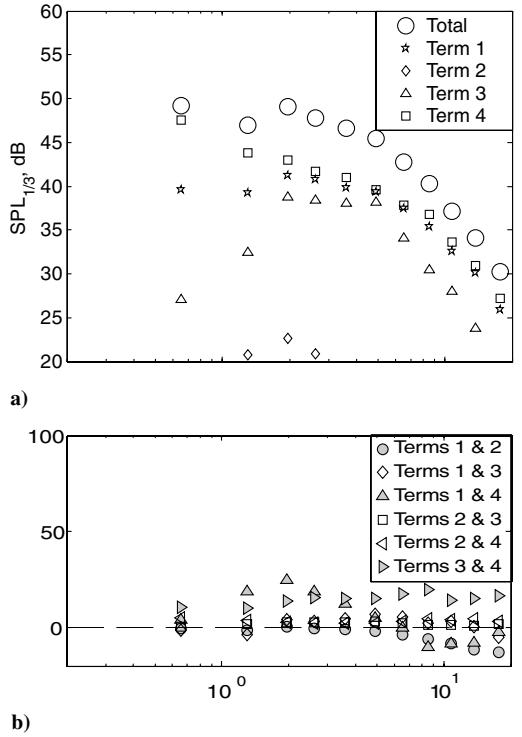

Fig. 5 Contributions to the predicted noise spectrum from the four terms: a) separate contributions, and b) contributions from products between terms as a percentage of total sound power.

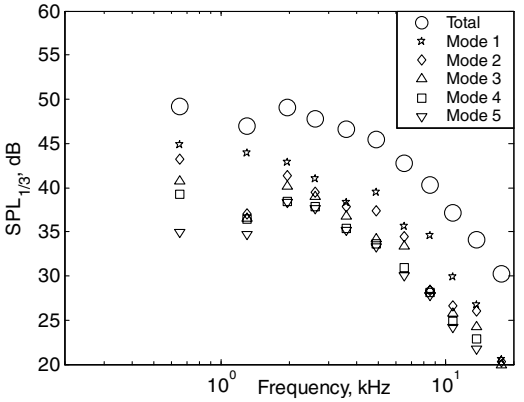

Fig. 6 Contributions to the predicted noise spectrum from the five most dominant modes in Eq. (12).

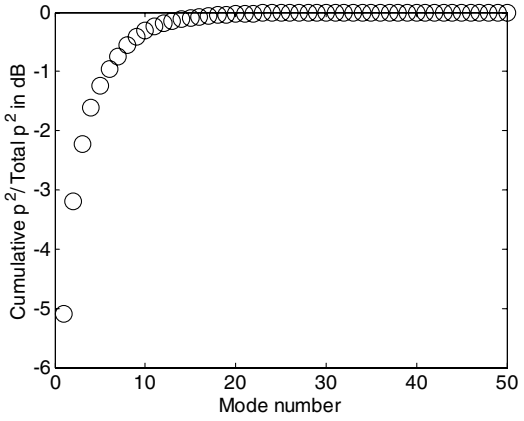

Fig. 7 Cumulative contribution to the predicted overall noise level as a function of mode number in Eq. (13).

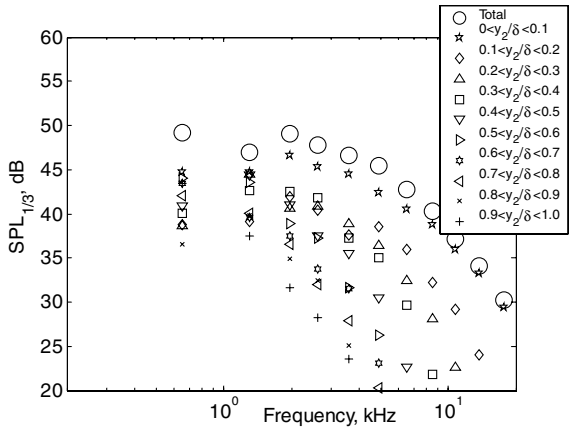

Fig. 8 Contributions to the predicted noise spectrum from different parts of the boundary layer.

(when combined with our earlier discussions) implies that the trailing-edge noise is primarily the result of large-scale motions in the near-wall region of the boundary layer. It is these motions that would therefore have to be captured by any fluid dynamic model used to provide velocity correlations for the purpose of computing trailing-edge noise using the present method.

VII. Conclusions

A new procedure for calculating trailing-edge noise from an airfoil by using detailed models of the turbulence in the blade boundary layer has been presented. The method has been applied to the

calculation of the noise produced by an isolated airfoil by using source terms extracted from the results of a DNS calculation. Comparison with experimental data shows the resulting predictions to be reasonably accurate, the largest discrepancies ($\sim$5 dB) occurring at frequencies where the DNS results are least applicable. An analysis of the prediction shows that most of the noise is produced by large-scale streamwise velocity modes in the bottom 10% of the boundary layer. About six modes at each frequency are needed to predict most of the noise produced.

Overall, the most important result of the present work is the predictive link it establishes between trailing-edge noise and modes of the turbulent velocity field near the trailing edge. This eliminates the need to estimate the surface pressure spectrum for trailing-edge noise calculations and relates the sound radiation directly to derivable flow parameters.

Acknowledgments

This work was supported under grants NAG-3-2702 and NAG-3-2710 from NASA John H. Glenn Research Center at Lewis Field, and the authors would like to thank Edmane Envia for his encouragement and support. The authors would also like to thank Robert Moser for his assistance in providing and explaining the direct numerical simulation data sets.

References

[1] Ffowcs Williams, J. E., and Hall, L. H., "Aerodynamic Sound Generation by Turbulent Flow in the Vicinity of a Scattering Half Plane," *Journal of Fluid Mechanics*, Vol. 40, No. 4, 1970, pp. 657–670. doi:10.1017/S0022112070000368

[2] Amiet, R. K., "Noise Due to Turbulent Flow Past a Trailing Edge," *Journal of Sound and Vibration*, Vol. 47, No. 3, 1976, pp. 387–393. doi:10.1016/0022-460X(76)90948-2

[3] Amiet, R. K., "Effect of the Incident Surface Pressure Field on Noise due to Turbulent Flow Past a Trailing Edge," *Journal of Sound and Vibration*, Vol. 57, No. 2, 1978, pp. 305–306. doi:10.1016/0022-460X(78)90588-6

[4] Howe, M. S., "A Review of the Theory of Trailing Edge Noise," *Journal of Sound and Vibration*, Vol. 61, No. 3, 1978, pp. 437–465. doi:10.1016/0022-460X(78)90391-7

[5] Howe, M. S., *Acoustics of Fluid Structure Interactions*, Cambridge Univ. Press, Cambridge, England, U.K., 1998.

[6] Glegg, S. A. L., and Jochault, C., "Broadband Self Noise from a Ducted Fan," *AIAA Journal*, Vol. 36, No. 8, Sept. 1998, pp. 1387–1395. doi:10.2514/2.559

[7] Glegg, S. A. L., and Devenport, W. J., "Proper Orthogonal Decomposition of Turbulent Flows for Aeroacoustic and Hydroacoustic Applications," *Journal of Sound and Vibration*, Vol. 239, No. 4, 2001, pp. 767–784. doi:10.1006/jsvi.2000.3128

[8] Freund, J. B., and Colonius, T., "POD Analysis of Sound Generation by a Turbulent Jet," AIAA Paper 2002-0072, 2002.

[9] Jordan, P., Schlegel, M., Stalnov, O., Noack, B., and Tinney, C. E., "Identifying Noisy and Quiet Modes in a Jet,"AIAA Paper 2007-3602, 2007.

[10] Tinney, C. E., Ukeiley, L. S., and Glauser, M. N., "Low-Dimensional Characteristics of a Transonic Jet, Part 2: Estimate and Far-Field Prediction," *Journal of Fluid Mechanics*, Vol. 615, 2008, pp. 53–92. doi:10.1017/S0022112008003601

[11] Moser, R. D., Kim, J., and Mansour, N. N., "Direct Numerical Simulation of a Turbulent Channel Flow up to $Re_\tau = 590$," *Physics of Fluids*, Vol. 11, No. 4, April 1999, pp. 943–945. doi:10.1063/1.869966

[12] Brooks, T. M., Pope, D. S., and Marcolini, M. A., "Airfoil Self Noise and Prediction," NASA RP 1218, 1989.

[13] Teitel, M., and Antonia, R. A., "Comparison Between Outer Regions of Turbulent Boundary Layer and Channel Flows," *Experiments in Fluids*, Vol. 11, Nos. 2–3, 1991, pp. 203–204.

[14] Teitel, M., and Antonia, R. A., "The Interaction Region in a Turbulent Duct Flow," *Physics of Fluids A*, Vol. 2, No. 5, 1990, pp. 808–813. doi:10.1063/1.857734

[15] Monty J. P, Stewart, J. A., Williams, R. C., and Chong, M. S., "Large Scale Features in Turbulent Pipe and Channel Flows," *Journal of Fluid Mechanics*, Vol. 589, 2007, pp. 147–156.

[16] Jimenez, J., "A Selection of Test Cases for the Validation of Large-Eddy Simulations of Turbulent Flows," AGARD, Advisory Rept. No. AGARD-AR-345, 1998.

M. Glauser
Associate Editor